

UDUC: An Uncertainty-driven Approach for Learning-based Robust Control

Yuan Zhang^{a,*}, Jasper Hoffman^a and Joschka Boedecker^a

^aNeurorobotics Lab, University of Freiburg, Germany

Abstract. Learning-based techniques have become popular in both model predictive control (MPC) and reinforcement learning (RL). Probabilistic ensemble (PE) models offer a promising approach for modelling system dynamics, showcasing the ability to capture uncertainty and scalability in high-dimensional control scenarios. However, PE models are susceptible to mode collapse, resulting in non-robust control when faced with environments slightly different from the training set. In this paper, we introduce the **uncertainty-driven robust control (UDUC)** loss as an alternative objective for training PE models, drawing inspiration from contrastive learning. We analyze the robustness of UDOC loss through the lens of robust optimization and evaluate its performance on the challenging Real-world Reinforcement Learning (RWRL) benchmark, which involves significant environmental mismatches between the training and testing environments.

1 Introduction

Traditional control methods usually require expert knowledge of the system to design controllers. However, with the development of deep learning algorithms and easy-to-access hardware resources, learning-based methods have attracted great interest in recent years. The common approach uses interactions with the environment to learn a model, which is further used to design controllers. Such data-driven approaches are often sample-efficient and thus popular in different research fields. Examples of this are learning-based model predictive control (LBMPC) [15] in the control community and model-based reinforcement learning (MBRL) in the reinforcement learning (RL) community.

The objective of those learning-based methods can be briefly expressed as learning a function $f(s'|s, a)$ to fit the transition distribution $\mathcal{T}(s'|s, a)$ with the sampled dataset, where s and s' are states and a is action. There are numerous ways to model the function f , e.g. parameterized physical function, Gaussian processes (GPs) [9], neural networks [23]. Among them, probabilistic ensemble (PE) models [8] $f(s'|s, a) = \frac{1}{B} \sum_{b=1}^B f_b(s'|s, a)$ can capture uncertainty in the system and scale with high-dimensional data. The structure of PE is flexible to be embedded into both LBMPC [8] and MBRL [17], thus being a promising modelling approach to be studied.

While PE-based methods have achieved great performance in simulated continuous control tasks (e.g. robotics), one potential concern to applying PE in real-world scenarios is its robustness. In detail, the data to train PE models usually comes from environments that are not the same as deployment. This mismatch is pervasive in control systems

and may be due to (1) parameter perturbation, e.g. damping and mass of the robots could change; (2) sim-to-real mismatch, when one learns models in simulation and directly applies in reality. In addition, the trained data is finite and will inevitably suffer from sampling error. As stated in Wang and Liu [34], a common concern is that the ensemble mode collapses, thus, multiple members converge to similar values, which is an undesirable case for robust control.

In this paper, we aim to promote the diversity of PE models for robust control inspired by the idea of contrastive learning (CL) [12]. The goal of CL is to learn such representation to effectively distinguish positive and negative samples. In the case of PE models, positive samples are collected from the training data, while negative samples are generated by other ensemble members. Intuitively, the model should learn to predict training data but be less similar to other members' predictions. We design a new loss function called **uncertainty-driven robust control (UDUC)** loss and explain the robustness of UDOC loss under training and testing mismatch in the view of robust optimization, based on previous study Wu et al. [37]. Furthermore, we evaluate UDOC on the Real-world Reinforcement Learning (RWRL) benchmark, demonstrating consistent improvements on perturbed testing environments, while only trained on one default training environment. Finally, we visualize the effects of UDOC loss to PE models on a physics-based function example.

2 Preliminaries

2.1 Probabilistic Ensemble Dynamics Models

A Markov decision process (MDP) [3] can be formulated as a 6-tuple $\langle \mathcal{S}, \mathcal{A}, \mathcal{T}, r, \mu_0, \gamma \rangle$. Here, \mathcal{S}, \mathcal{A} represent the state and action space respectively, $\Delta_{\mathcal{S}}$ and $\Delta_{\mathcal{A}}$ the space of probability measures over \mathcal{S} and \mathcal{A} , and $r(s, a) : \mathcal{S} \times \mathcal{A} \rightarrow \mathbb{R}$ the reward function. The initial state is sampled from an initial distribution $\mu_0 : \Delta_{\mathcal{S}}$, and the future rewards are discounted by the discount factor $\gamma \in [0, 1]$. The transition function $\mathcal{T}(s'|s, a) : \mathcal{S} \times \mathcal{A} \rightarrow \Delta_{\mathcal{S}}$ provides a probability distribution of the next state given the current state and action. For the real system, the exact form of the transition function is usually unknown; instead, the sampled measurements $\mathcal{D} = \{s_i, a_i, s'_i\}_{i=1}^N$ can be accessed from interactions. It's a common practice to learn the transition function $f : \mathcal{S} \times \mathcal{A} \rightarrow \Delta_{\mathcal{S}}$ by fitting the dataset \mathcal{D} , which can be further utilized by various model predictive control (MPC) [5] or reinforcement learning (RL) [30] methods, referred to popular research directions as learning-based MPC [15] and model-based RL [35].

There are plenty of ways to model the transition function f . Among them, probabilistic ensemble (PE) models [8] can handle

* Corresponding Author. Email: yzhang@cs.uni-freiburg.de.

both aleatoric and epistemic uncertainty (due to the inherent stochasticity of the system and limited data respectively) and scale well with high-dimensional data. PE consists of B probabilistic models. Each model f_b is a Gaussian distribution: $f_b(s'|s, a; \theta_b) = \mathcal{N}(\mu(s, a; \theta_b), \Sigma(s, a; \theta_b))$ for its power of expression in continuous space, where $\mu : S \times A \rightarrow S$ and $\Sigma : S \times A \rightarrow S^2$ are two neural networks parameterized with θ_b to predict the mean and covariance of the next state s' . The final structure of a PE is $f(s'|s, a; \theta) = \frac{1}{B} \sum_{b=1}^B f_b(s'|s, a; \theta_b)$, where $\theta = \{\theta_1, \theta_2, \dots, \theta_B\}$. Each model f_b is trained on a sub-dataset \mathcal{D}_b , generated by independently sampling N samples (with replacement) from the large dataset \mathcal{D} . For each sample (s, a, s') in \mathcal{D}_b , the loss function for model b is essentially the negative log-likelihood:

$$\begin{aligned} \mathcal{L}_{\text{PE}}(\theta_b, s, a, s') &= -\log P(s'|s, a; \theta_b) \\ &= [\mu(s, a; \theta_b) - s']^T \Sigma^{-1}(s, a; \theta_b) [\mu(s, a; \theta_b) - s'] \\ &\quad + \log \det \Sigma(s, a; \theta_b). \end{aligned} \quad (1)$$

Therefore, the final loss for model b is the average over samples: $\mathcal{L}(\theta_b, \mathcal{D}_b) = \frac{1}{N} \sum_{i=1}^N \mathcal{L}_{\text{PE}}(\theta_b, s_i, a_i, s'_i)$. After all B models have been trained, one can use the ensemble models by the trajectory sampling method [8]. Specifically speaking, to predict the next state s' at each state-action pair (s, a) , one model b is uniformly selected from the ensemble models, and the next state s' is drawn from the Gaussian distribution $f_b(s'|s, a; \theta_b)$. This propagation method is shown to best preserve the multimodality of the ensemble models, which plays a crucial role in the robustness.

2.2 Contrastive Learning

Contrastive learning (CL) is widely adopted in the computer vision realm [7, 14, 6], aiming to gather images within the same class (positive samples) and distinguish dissimilar ones (negative samples) on an abstract embedding vector space. In this paper, we primarily focus on InfoNCE loss [33] as the learning objective. Given a context vector c , one positive sample x^+ is drawn from the distribution $p(x|c)$, which describes the natural probability relationship between x and c . Another $K-1$ negative samples are drawn from $q(x)$, which is a distribution independent of c . The positive and negative samples together form the sample set $\mathcal{X} = \{x_1, \dots, x_K\}$. The motivation of InfoNCE loss is to learn a representative function $g_\theta(x, c)$, parameterized with θ , to preserve the mutual information between the sample x and the context c , which specifically has the following form:

$$\mathcal{L}_{\text{InfoNCE}}(\theta, \mathcal{X}, c) = -\log \frac{\exp(g_\theta(x^+, c)/\tau)}{\sum_{x \in \mathcal{X}} \exp(g_\theta(x, c)/\tau)}, \quad (2)$$

where the temperature τ is a key hyperparameter in InfoNCE loss to learn robust representation against sampling bias, as studied in recent work [37]. The optimal solution satisfies that $g_\theta(x, c) = \log \frac{p(x|c)}{q(x)} + \text{const}$, as claimed by van den Oord et al. [33]. Besides, He et al. [14] suggest using a slowly-updated target network $g_{\bar{\theta}}$ to replace the network g_θ in Equation 2's denominator for a stable learning process. As suggested in [37], InfoNCE loss can be written in the expectation form as $\mathcal{L}_{\text{InfoNCE-e}}(\theta, c) = -\log \frac{\mathbb{E}_{x^+ \sim p(x|c)}[\exp(g_\theta(x^+, c)/\tau)]}{\mathbb{E}_{x \sim q(x)}[\exp(g_\theta(x, c)/\tau)]}$, which is convenient for theoretical analysis.

3 UDUC: Uncertainty-driven Robust Control

The ensemble dynamics models introduced in Section 2.1 often fail to be applied to real-world robots, and require other advanced tech-

niques like meta reinforcement learning [24] to fine-tune the model parameters and improve the performance. The failure results from the mismatch between training and deployment environments and the vulnerable robustness of the ensemble functions. In this section, we introduce how to build on the idea of contrastive learning (CL) and improve the robustness of the ensemble functions.

Generally speaking, we enhance the standard training objectives of the probabilistic ensemble functions introduced in Section 2.1 with an auxiliary CL objective. The contrastive learning objective builds on InfoNCE loss by contrasting the real next observations to the virtual next observations generated by other ensemble functions. Intuitively, this loss aims to increase the uncertainty among ensemble members' predictions and thus better apply to perturbed environments, so-called **Uncertainty-driven Robust Control (UDUC)** loss. We first introduce the specific procedures to implement UDUC loss, and further theoretically analyze it in the view of robust optimization. Finally, we provide a practical robust control approach combined with both RL-based and optimization-based controllers.

3.1 Implementing UDUC Loss

Figure 1 depicts the overall procedures to implement UDUC loss. As the setup in Section 2.1, there are B ensemble models and each model $f_b(s'|s, a; \theta_b)$ is a Gaussian distribution on the next state s' . Each model maintains its own replay buffer \mathcal{D}_b . For a single sample (s, a, s') drawn from this replay buffer, considering the current state-action pair (s, a) as context c and the next state s' as sample x , one can directly construct a positive sample s'_b by cloning s' . $B-1$ negative samples can be generated by forward passing (s, a) to other $B-1$ ensemble functions (except for model b) and sampling the next states from these Gaussian distributions $f_i(s'|s, a; \theta_i)$, $\forall i \neq b$. Gathering all positive and negative samples returns a sample set $\mathcal{X} = \{s'_1, \dots, s'_B\}$. Replacing $g_\theta(x, c)$ in InfoNCE loss (Equation 2) by $-\mathcal{L}_{\text{PE}}(\theta_b, s, a, s')$, UDUC loss can be thus obtained:

$$\begin{aligned} \mathcal{L}_{\text{UDUC}}(\theta_b, s, a, \mathcal{X}) &= (1 - \frac{1}{\tau}) \mathcal{L}_{\text{PE}}(\theta_b, s, a, s'_b) + \mathcal{L}_{\text{InfoNCE}}(\theta_b, s, a, \mathcal{X}) \\ &= (1 - \frac{1}{\tau}) \mathcal{L}_{\text{PE}}(\theta_b, s, a, s'_b) - \log \frac{\exp(-\mathcal{L}_{\text{PE}}(\theta_b, s, a, s'_b)/\tau)}{\sum_{s' \in \mathcal{X}} \exp(-\mathcal{L}_{\text{PE}}(\theta_b, s, a, s')/\tau)} \\ &= \mathcal{L}_{\text{PE}}(\theta_b, s, a, s'_b) + \log \sum_{s' \in \mathcal{X}} \exp(-\mathcal{L}_{\text{PE}}(\theta_b, s, a, s')/\tau). \end{aligned} \quad (3)$$

The final loss for model b is the average over samples: $\mathcal{L}(\theta_b, \mathcal{D}_b) = \frac{1}{N} \sum_{i=1}^N \mathcal{L}_{\text{UDUC}}(\theta_b, s_i, a_i, \mathcal{X}_i)$. Intuitively, $\log \sum_{s' \in \mathcal{X}} \exp(-\frac{1}{\tau} \mathcal{L}_{\text{PE}}(\theta_b, s, a, s'))$ is the additional term apart from the standard PE loss when training the ensemble functions. This term can be interpreted as a regularizer that encourages the model b to predict less similar samples to other ensemble members. Therefore, a more diverse set of transition functions is achieved and can function like domain randomization (DR) approaches [25] to trigger more robust controllers against diverse transitions. In comparison, DR randomly initializes multiple environments with various physical environmental parameters, while our method learns diverse virtual transition functions in one single training environment. This makes our method less resource-consuming and less expert knowledge required to achieve robust policies.

In practice, we use a target network [14] for each model b with the Gaussian distribution $f_b(s'|s, a; \theta_b)$ to generate negative samples for the sample set \mathcal{X} . The target network is updated slower than the true parameter θ_b with $\bar{\theta}_b = \rho \theta_b + (1-\rho) \bar{\theta}_b$, to stabilize the learning process. Besides, when updating model b , the sample set \mathcal{X} also includes the

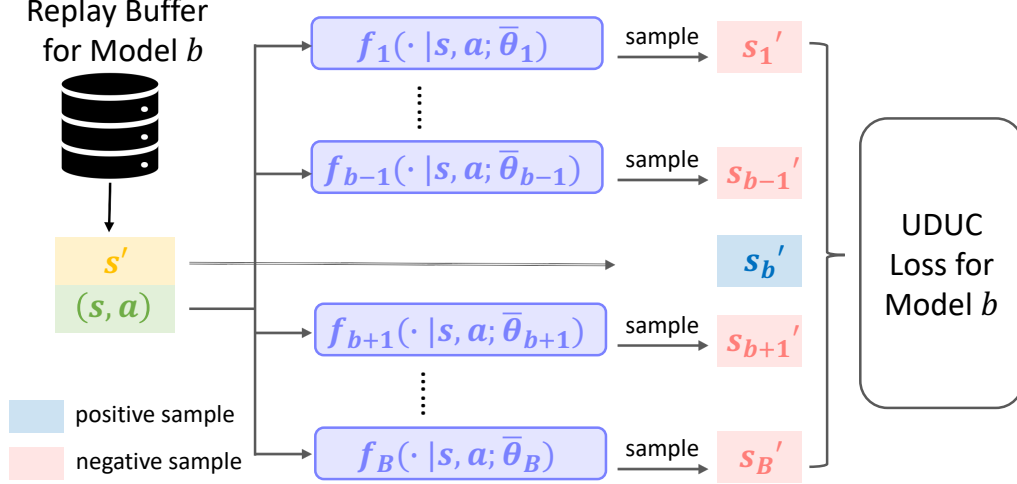


Figure 1: The overall procedure to implement UDUC loss on ensemble functions.

sample s' generated from its own target network $f_b(s'|s, a; \bar{\theta}_b)$, which we call it "self-regularization". This term can be understood as the model b also contrasts its past predictions generated by its target network. This essentially provides a larger set of transitions for more robust controllers, empirically shown in Section 4.3.

3.2 Understanding UDUC loss

In this section, we rethink UDUC loss proposed in Equation 3 with the view of robust optimization to understand its effect in detail. In the case of UDUC loss, we first denote the training environment's transition distribution $\mathcal{T}_{\text{train}}(s'|s, a)$ ($\mathcal{T}_{\text{train}}$ in short), possible testing environment's transition distribution $\mathcal{T}_{\text{test}}(s'|s, a)$ ($\mathcal{T}_{\text{test}}$ in short) and probabilistic ensemble functions with target parameters $f(s'|s, a; \bar{\theta}) = \frac{1}{B} \sum_{b=1}^B f_b(s'|s, a; \bar{\theta}_b)$. When utilizing the learned ensemble models, the next state s' is sampled from the distribution $f(s'|s, a; \bar{\theta})$, on which the control methods (MPC, RL) can make further plannings. The control is effective on the unseen testing environment $\mathcal{T}_{\text{test}}$ if the difference of the log-likelihood on these two distributions is low, i.e. $\mathbb{E}_{s' \sim f(s'|s, a; \bar{\theta})} [-\mathcal{L}_{\text{PE}}(\theta_b, s, a, s')] - \mathbb{E}_{s' \sim \mathcal{T}_{\text{test}}} [-\mathcal{L}_{\text{PE}}(\theta_b, s, a, s')] \rightarrow 0$. Intuitively, this difference can be used as a regularization term of θ_b to improve its robustness in unseen environments. We formally formulate the above idea as a robust optimization problem and prove its equivalence to UDUC loss (Equation 3) in the following Proposition.

Proposition 1 (Understanding UDUC loss). *Minimizing UDUC loss is equivalent to the following robust optimization problem:*

$$\begin{aligned} \min_{\theta_b} \mathcal{L}_{\text{RO}}(\theta_b, s, a) = & \min_{\theta_b} \left(1 - \frac{1}{\tau} \underbrace{\mathbb{E}_{s' \sim \mathcal{T}_{\text{train}}} [\mathcal{L}_{\text{PE}}(\theta_b, s, a, s')]}_{\text{negative log-likelihood term}} \right) \\ & + \frac{1}{\tau} \underbrace{\left(\mathbb{E}_{s' \sim f(s'|s, a; \bar{\theta})} [-\mathcal{L}_{\text{PE}}(\theta_b, s, a, s')] - \max_{\mathcal{T}_{\text{test}}} \mathbb{E}_{s' \sim \mathcal{T}_{\text{test}}} [-\mathcal{L}_{\text{PE}}(\theta_b, s, a, s')] \right)}_{\text{regularization term}} \end{aligned}$$

$$s.t. \quad D_{\text{KL}}(\mathcal{T}_{\text{test}} || \mathcal{T}_{\text{train}}) \leq \eta, \eta \approx \mathbb{V}_{s' \sim f(s'|s, a)} [\mathcal{L}_{\text{PE}}(\theta_b, s, a, s')] / 2\tau^2.$$

$\mathcal{L}_{\text{RO}}(\theta_b, s, a)$ is the target of this robust optimization problem, consisting of a negative log-likelihood term and a regularization term. The detailed proof is built on top of Wu et al. [37] and can be found in Section A.1. Intuitively, Proposition 1 shows that UDUC loss is equivalent to a robust optimization problem with two targets. The negative log-likelihood term fits training environment $\mathcal{T}_{\text{train}}$ as the normal

objective in previous work. The regularization term itself is a robust optimization objective, which aims to minimize the predictive probability ($\mathcal{L}_{\text{PE}}(\theta_b, s, a, s')$) between samples generated by the learned function $f(s'|s, a; \bar{\theta})$ and testing environment $\mathcal{T}_{\text{test}}$, within the neighbourhood of $\mathcal{T}_{\text{train}}$ (measured by the KL divergence). Accordingly, the distribution shift between these two transitions can be largely eased due to this regularization term. In addition, the temperature τ in InfoNCE loss is inversely proportional to the robust radius η , implying that smaller values of τ , as an important trade-off factor, can induce larger robustness but also impact the performance on nominal training environment $\mathcal{T}_{\text{train}}$.

3.3 Practical Robust Control Approach

The proposed UDUC loss is flexible to be plugged into both MBRL and LBMPC algorithms to improve the robustness of the controllers. Here we introduce the detailed process in Algorithm 1. Line 7 to 12 denote the model update process, which essentially utilizes UDUC loss to learn parameters θ . Line 13 to 15 update the agent with the model dataset $\mathcal{D}_{\text{model}}$ generated by transition function $f(s'|s, a; \bar{\theta})$. Notably, this step can be omitted for MPC methods (e.g. CEM [28]) since it directly utilizes transition function $f(s'|s, a; \bar{\theta})$ for control. For neural-network-policy $\pi(a|s)$ in RL, any standard on-policy and off-policy algorithms (e.g. SAC [13], PPO [29]) can be adopted to improve the policy. Notably, both MBRL and LBMPC necessitate the utilization of transition function $f(s'|s, a; \bar{\theta})$ to rollout the trajectory. As introduced in Section 2.1, we adopt the trajectory sampling approach by randomly selecting one model b among all ensembles at each step and sampling next state s' from the Gaussian distribution $f(s'|s, a; \bar{\theta}_b)$. The trajectory sampling approach is considered to maintain the multimodality of the trajectory [17], which is necessary to generate diverse samples as motivated by UDUC loss. The detailed procedures to construct control policies with probabilistic ensemble functions for both MPC and RL are explained in Appendix A.2.

4 Experiments

In this section, we evaluate the robustness of the UDUC-based methods on the Real-world Reinforcement Learning (RWRL) benchmark [10]. Afterwards, we analyze the experimental results by visualizing the model parameters on the cart-pole [2] environment.

Table 1: Tasks in RWRL benchmark and their modified physical parameters. The function $\text{linspace}(a, b, n)$ returns n values evenly spaced over $[a, b]$.

Task Name	$\text{dim}(S)$	$\text{dim}(A)$	Modified parameters	Training Values	Testing Values
walker_stand walker_walk	24	6	thigh length torso length joint damping contact friction	0.225 0.3 0.1 0.7	$\text{linspace}(0.1, 0.7, 20)$ $\text{linspace}(0.1, 0.7, 20)$ $\text{linspace}(0.1, 10.0, 20)$ $\text{linspace}(0.01, 2.0, 20)$
humanoid_walk	45	17	head size contact friction joint damping	0.09 1.0 1.0	$\text{linspace}(0.01, 0.19, 20)$ $\text{linspace}(0.01, 2.5, 20)$ $\text{linspace}(0.05, 1.2, 20)$

Algorithm 1 UDUC Algorithm

- 1: **Input:** ensemble transition function $f(s'|s, a; \theta)$ with parameters $\theta = \{\theta_1, \dots, \theta_B\}$, policy function $\pi(a|s)$, environment dataset $\mathcal{D}_{\text{env}} = \{\}$, model dataset $\mathcal{D}_{\text{model}} = \{\}$, target update rate ρ , initial state s , model-agent update frequency F_{model} and F_{agent}
- 2: Set target transition function's parameters $\bar{\theta} \leftarrow \theta$
- 3: **for** steps $i = 1, 2, \dots$ **do**
- 4: Execute $a \sim \pi(a|s)$ in the training environment
- 5: Observe reward r and next state s'
- 6: $\mathcal{D}_{\text{env}} \leftarrow \mathcal{D}_{\text{env}} \cup \{s, a, r, s'\}$ and $s \leftarrow s'$
- 7: **if** $i \bmod F_{\text{model}} \equiv 0$ /*update model*/ **then**
- 8: Update parameters θ by minimizing Equation 3
- 9: Update target parameters $\bar{\theta} \leftarrow (1 - \rho)\bar{\theta} + \rho\theta$
- 10: Rollout transitions $(s_n, a_n, r_n, s_{n+1})_{n=1}^N$ with $f(s'|s, a; \bar{\theta})$, $\pi(a|s)$ and $r(s, a)^1$
- 11: Store in the model dataset $\mathcal{D}_{\text{model}} \leftarrow \mathcal{D}_{\text{model}} \cup \{(s_n, a_n, r_n, s_{n+1})_{n=1}^N\}$
- 12: **end if**
- 13: **if** $i \bmod F_{\text{agent}} \equiv 0$ /*update agent*/ **then**
- 14: Update $\pi(a|s)$ with $\mathcal{D}_{\text{model}}$ and preferred algorithms (e.g. SAC approach [13] in RL) if needed
- 15: **end if**
- 16: **end for**

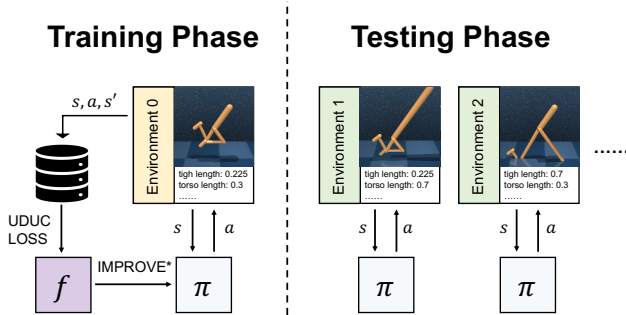


Figure 2: Visualization on the task setup. Notably, only one default environment is available during training, while the learned policy is evaluated on multiple varied testing environments. The approach to improve policy π from learned transition function f depends on specific algorithms, e.g. SAC [13] for reinforcement learning, CEM [28] for model predictive control.

4.1 Experimental Setups

Task setup RWRL is a continuous control benchmark for robotics, featuring multiple real-world challenges for RL algorithms, e.g. robustness, delays and safety. The physics simulator of RWRL is

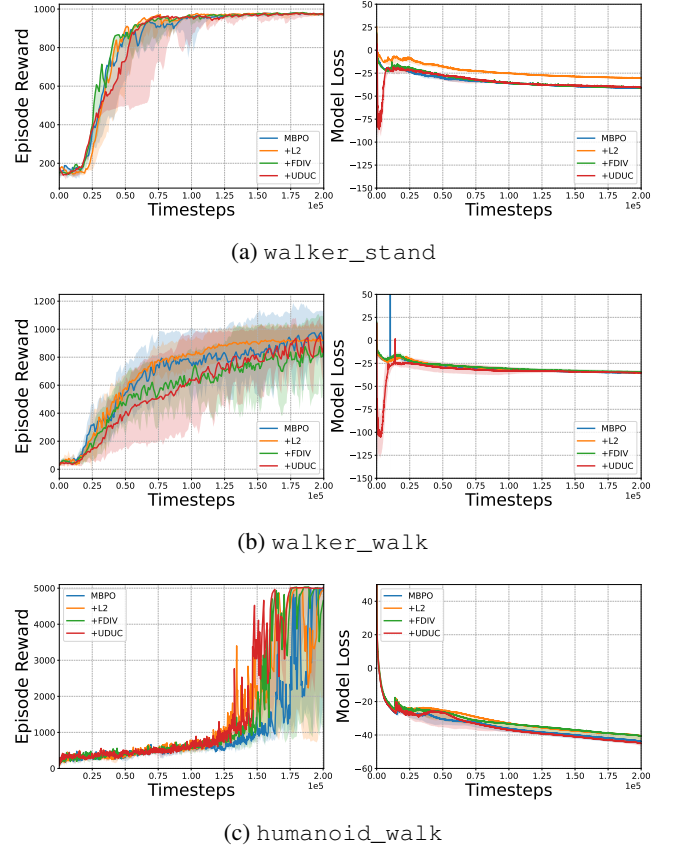


Figure 3: Training curves on robot control tasks. The x-axis is the environment time steps and the y-axis is the sum of rewards for each episode and the training loss for ensemble functions. All graphs are plotted with median and 25%-75% percentile shading across 5 seeds.

grounded on the MuJoCo engine [32]. Upon this benchmark, we first train all model-based baselines on the nominal environment with default physical parameters, where the transition distribution is denoted as $\mathcal{T}_{\text{train}}(s'|s, a)$. Afterwards, some physical parameters are modified and therefore a set of testing environments is formalized. For each testing environment with the transition distribution $\mathcal{T}_{\text{test}}(s'|s, a)$, all trained baselines are tested on it without any fine-tuning, aiming to indicate the robustness against the mismatch in transition distributions.

In this paper, we conduct experiments on 2 robots (walker and humanoid) with 3 tasks: walker_stand, walker_walk, humanoid_walk, with growing complexity in state and action space. The modified physical parameters and their values can be found in Table 1. The range of the testing values significantly exceeds

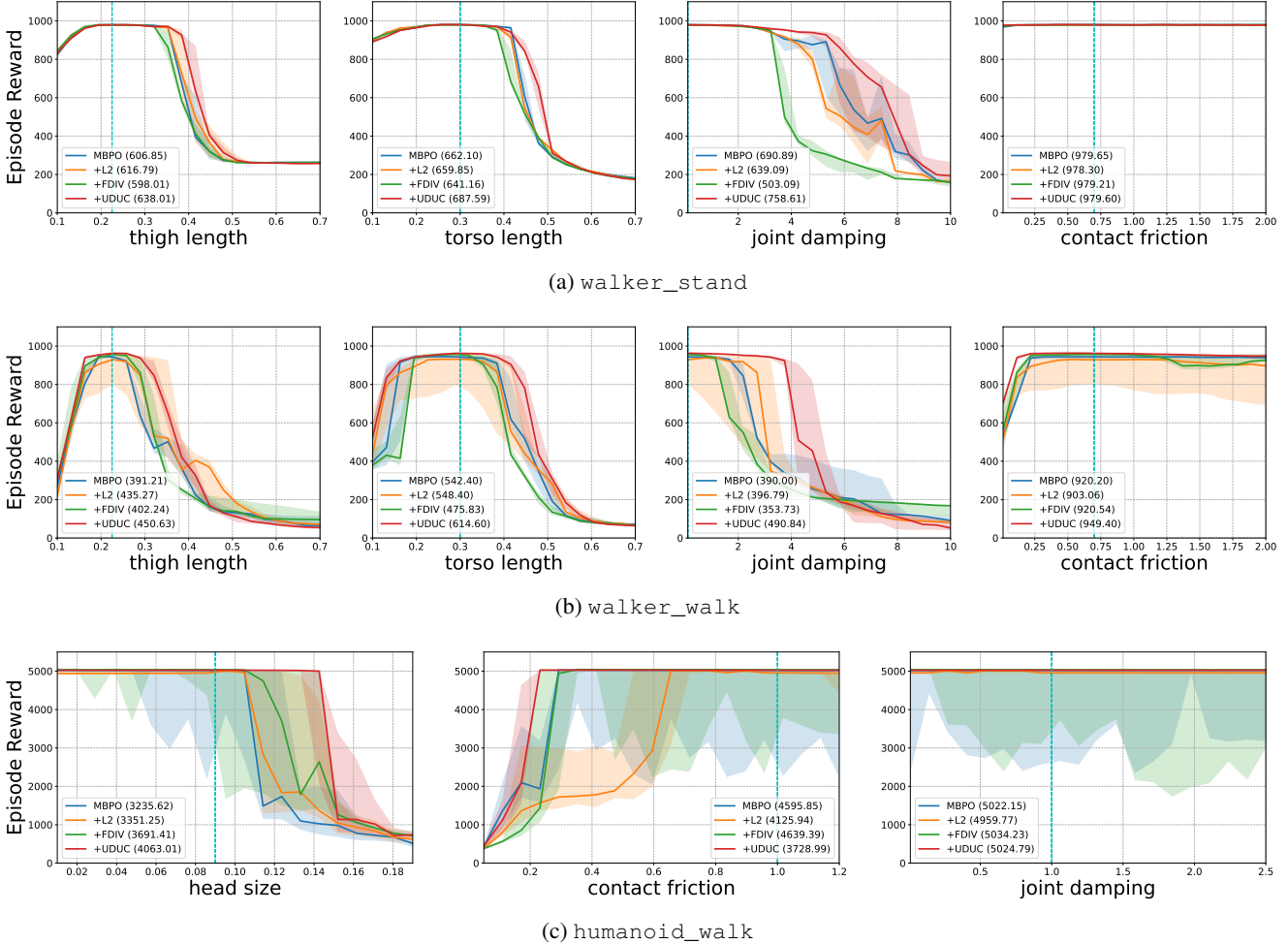


Figure 4: Testing curves on robot control tasks. The x-axis is the values of perturbed physical parameters and the y-axis is the episodic reward under the perturbed environments. The vertical dashed line denotes the nominal value during training. All graphs are plotted with the median and 25%-75%-quantile shading by running on 100 episodes. Robust-AUC is illustrated after each label in the graph.

that of the training values, making the testing environments challenging. The details of the robots and tasks are introduced in Appendix B.1. We further exemplify the task setup in Figure 2. During training, the transition f learns the dynamics of the default walker robot and the policy π learns to make the robot stand with the knowledge of f . During testing, the walker robot’s physical parameters (e.g. thigh length, torso length) have been changed, and the learned policy π is directly tested on those modified environments without tuning.

Baselines We consider model-based RL algorithms as baselines in this section. Viewing UDUC loss as an approach to regularize the model learning, we include other regularization approaches to compare their robustness.

- MBPO: a model-based RL approach which combines probabilistic ensemble functions for transition modelling and SAC [13] for policy improvement. This baseline is adopted to indicate the performance without regularization techniques;
- MBPO + L2: an L_2 -norm regularization is added in the model training process, expressed as $\mathcal{L}(\theta) = \sqrt{\theta^T \theta}$. L_2 -norm regularization is proved to be one of the simplest and the most effective regularization methods in RL research [21];
- MBPO + FDIV: an objective to minimize the f -divergence [31]

is performed on learning ensemble functions. Notably, the work also aims to promote the diversity of ensemble functions but only regulates the mean predictions;

- MBPO + UDUC: it follows Algorithm 1 to minimize UDUC loss when training models and adopts SAC to learn policy $\pi(a|s)$ at the same time.

All baselines adopt the same neural network architectures as ensemble functions. The hyperparameters of all baselines are set equally for fair comparison, except for the regularization coefficients, which are tuned accordingly. The specific setups are clarified in Appendix B.2.

4.2 Main Results

We first demonstrate the training performances in Figure 3. Since all baselines are trained on the same default environment, they converge to almost the same episode reward in the end. Notably, at the early stage of training a walker robot, UDUC loss learns slower than baselines and indicates a larger uncertainty. At this stage, the diversity part of UDUC loss overwhelms the part of imitating the default environment, which is also shown in the curve of model loss that there is a dent at the beginning. For more complex robots like humanoids, regularization itself can benefit from reducing unnecessary information

and speeding up the training process. A more detailed analysis of the training process is delivered in Appendix C.1.

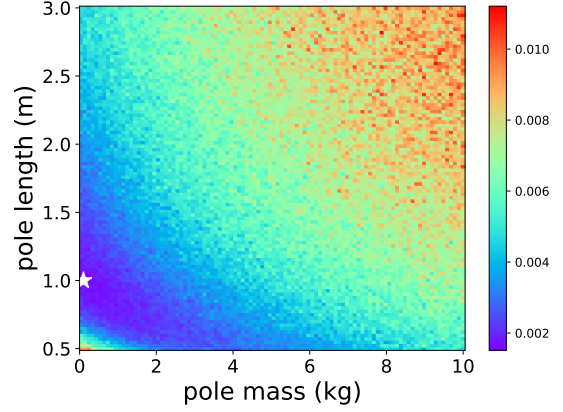
Moving on to the testing phase, we organize evaluation results by different physical parameters as Figure 4. We can first observe that the control performances become worse for all agents as the physical parameter deviates from the training value. Importantly, UDUC stays on top of other baselines for most of the time, indicating more robust control performance under various testing environments. Inspired by Zhang et al. [38], we measure the robustness numerically with the metric Robust-AUC (noted in brackets in the legend), which is calculated as the relative area under the curve of the episode reward to the perturbed physical parameters. The Robust-AUC of UDUC clearly outperforms other baselines, especially for physical parameters that have large influences on the dynamics (e.g. joint damping in the walker robot and head size on the humanoid robot). Notably, L2 and FDIV regularizations only improve the robustness in a few cases, but sometimes even impair the performance in comparison with the non-regularised agent on simple domains.

4.3 Ablation Study

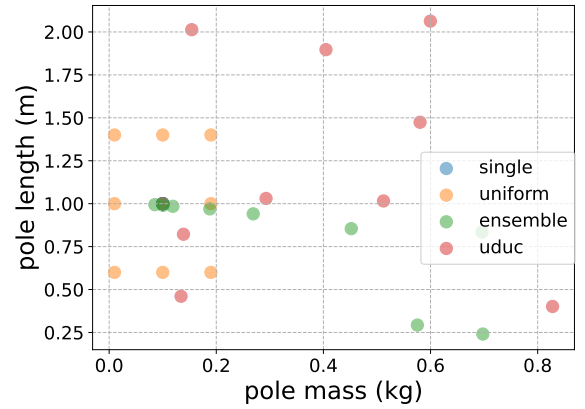
To fully understand why UDUC loss can provide additional robustness in complex continuous control tasks, we visualize the learning outcomes of UDUC loss on a toy example in this section. Specifically, we would like to answer the following questions: (1) what is the distribution of the learned model parameters? (2) how does the temperature τ act on the robustness? (3) does the self-regularization promote overall diversity? (4) do more ensemble members bring more robustness?

Task setup For this toy example, we select the task of balancing a cart-pole with varying mass m and length l [4]. The environment has a 4-dim state space and a 1-dim action space. The reward is 1 for an upright state otherwise 0. The maximum episode length is 100. Suppose the task holds a fixed noise, and its true dynamics with $f_t(s'|s, a; m, l)$ are determined by the mass and length, for simplicity of analysis, we directly assign the probabilistic ensemble model b the same structure $f_b(s'|s, a; \theta_b) = f_t(s'|s, a; m_b, l_b)$ with parameters $\theta_b = (m_b, l_b)$ to learn. To avoid the influence of other learning processes, we adopt an MPC-based approach for control (see Appendix A.2.1 for details). The number of ensemble members $B = 9$ and temperature $\tau = 1$ unless otherwise stated. The environmental parameters are set to $m = 0.1, l = 1.0$ for training, and $m \in [0.05, 10.0], l \in [0.3, 3.0]$ for testing.

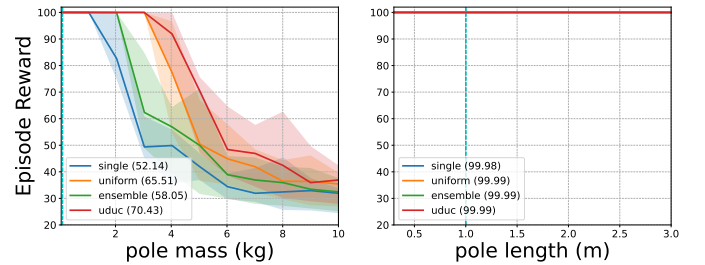
Learned parameters Since we adopt the physical functions as the ensemble functions, we can directly visualize the learned parameters in Figure 5b. The compared methods are (i) ensemble functions trained with negative log-likelihood only ("ensemble"); (ii) all 9 ensemble members are set to the same parameters as the training environment ("single") (iii) all 9 ensemble members are evenly distributed on the parameter space ("uniform"), centering on the training parameter. It can be observed that UDUC loss learns more diverse parameters and occupies larger parameter space compared with other baselines. Figure 5a tells the prediction mismatch between training (marked in star) and testing environments for reference, which is calculated by $\mathbb{E}_{s,a}[(f_t(s, a; m_{\text{train}}, l_{\text{train}}) - f_t(s, a; m_{\text{test}}, l_{\text{test}}))^2]$, where s, a are randomly sampled from the state and action space. There is a larger mismatch in the top right corner, and only UDUC loss learns members in this region. Combined with the utilization of the trajectory sampling approach (introduced in Section 3.3), there exists the potential for controllers to encounter transitions from this region, leading to robust performance under testing with unseen environmental parameters.



(a) The average prediction error on states between training and testing physical parameters. The error is averaged over 100 random predictions. The star represents the training parameter.



(b) The learned parameters of the physical ensemble functions. There are 9 points for each method.



(c) Testing curves on the cart-pole balance task, which has the same format as Figure 4.

Figure 5: Testing analysis on the cart-pole balance task.

We further plot the testing curves in Figure 5c. Both the curve and Robust-AUC value indicate that UDUC loss learns more robust ensemble parameters. More interestingly, the two physical parameters influence the robustness at different levels. UDUC pays more attention to pole mass with members ~ 8 times training values in the pole mass parameter, while ~ 2 times in the pole length parameter.

Temperature τ As explained in Section 3.2, the temperature τ in UDUC loss is connected with the robust radius η of the dynamics mismatch. As the temperature decreases, the corresponding robust optimization problem exhibits an increase in robust radius, which also means the solutions could be more conservative. We calculate the

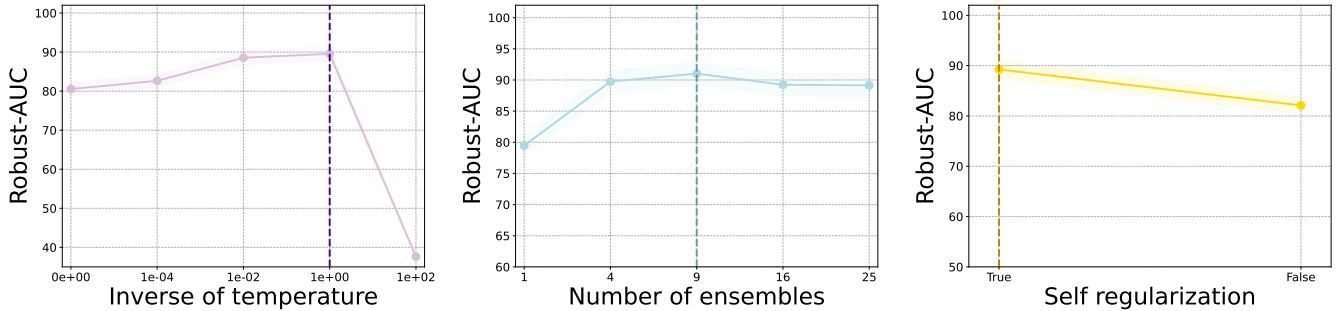


Figure 6: Robust-AUC w.r.t. different designs of UDUC loss.

Robust-AUC under different values of temperature τ and plot on the left of Figure 6. Notably, the x -axis is the inverse of temperature τ , which is proportional to the robust radius η . There exists a sweet spot in the temperature, meaning it doesn't impact the control performance too much but could maintain a larger range of robustness.

Number of ensemble members B We plot how the robustness is influenced by the number of ensemble functions in the middle of Figure 6. As the number of ensemble members increases, the robustness increases at the beginning and gradually saturates. Ideally, more ensemble members can occupy more parameter space, but it could burden the training of UDUC loss by contrasting in too many directions.

Regularization on self-prediction As introduced in Section 3.1, UDUC loss utilizes the technique of "self-regularization" in practice, which adds the own predictions from $f(s'|s, a; \bar{\theta}_b)$ to regulate the learning of model b . Most previous related work [34, 31] remove this term from regularizers for pure negative samples. However, Wu et al. [37] demonstrates that InfoNCE loss can gain additional robustness from the self-regularization term under the appropriate temperature, which is also true for UDUC loss. The right result of Figure 6 shows that self-regularization does help the overall performance. It can be understood in a way that the member i also contrasts its past prediction generated by its target network. This essentially provides a larger set of transitions, resulting in more robust controllers.

The key takeaways from the ablation study are as follows: self-regularization and the use of a large number of ensemble models are crucial for enhancing the robustness of the controller. Additionally, the temperature parameter needs to be carefully tuned, as discussed in Section B.2.

5 Related Work

Robustness is a fundamental dimension to evaluate a control method since real-world systems are usually noisy and non-stationary. This topic is well-studied in both Optimal Control (OC) [1] and Reinforcement Learning (RL) [16, 36, 22, 38] fields. The overall vision is to derive a control policy $\pi^*(a|s)$ that can resist the perturbations in the transition function $\mathcal{T} \in \mathbb{T}$. In mathematics, it is equivalent to $\pi^* = \operatorname{argmax}_{\pi} \min_{\mathcal{T} \in \mathbb{T}} \mathbb{E}_{\pi, \mathcal{T}} [\sum_{t=0}^{+\infty} \gamma^t r(s_t, a_t)]$. With the recent successes in the field of machine learning, it becomes practical and promising to learn transition functions $f(s'|s, a; \theta)$ from the data, and apply such functions to achieve the final control policy $\pi(a|s)$, denoted as Model-based RL (MBRL) and Learning-based Control (LBC) in both fields. As a result, the policy is strongly related to the parameters θ of the transition functions, raising a great concern to learn both accurate and robust transition functions, which directly

motivates this research.

Regularization plays a key role in improving the robustness of learning-based methods. The Euclidean norm is one of the most widely applied regularization methods, which also dominates the learning of policy functions in the field of RL [21]. However, as shown in Section 4, it fails to maintain robustness on probabilistic ensemble transition functions, which is one of the state-of-the-art modelling approaches to capture both epistemic uncertainty and aleatoric uncertainty. A line of work strives to promote diversity for ensemble learning [34, 18, 27, 26, 31]. Unlike InfoNCE considering all ensemble members' predictions, most of these methods exclude the predictions of the trained member when calculating the diversity regularization. This could lead to a smaller robust radius under perturbed testing environments, which is analyzed in Section 4.3. We select a representative and concise work Tiulpin and Blaschko [31] among them as baselines in the experiments. This work manages to increase the diversity of deep ensembles by the marginal gain on the negative f -divergence, without heavy adversarial dataset [18, 27] or expensive generative models [26].

Contrastive learning has been involved in the RL field recently. CURL [20] contrasts different images with InfoNCE loss [33] and momentum target [14] to learn a representative low-level space for further controls. The success of CURL is strongly related to better image embedding and less on the control rule itself. Eysenbach et al. [11] maximizes the mutual information between states and skills by contrasting randomly sampled skills and encourages the agents to explore the uncovered skills, which mainly promotes the exploration but not robustness.

6 Conclusion

In conclusion, in this paper, we propose UDUC loss as an alternative objective to train probabilistic ensemble transition models inspired by InfoNCE loss. The diverse transition models can further enhance the robust control performance, which can be understood from domain randomization and robust optimization perspectives. Furthermore, we evaluate the robustness of UDUC on the challenging RWRL benchmark, where large environmental mismatches exist, and UDUC can consistently lead to more robust controllers.

For future work, we plan to validate UDUC with a more diverse set of low-level control algorithms, including the optimization-based optimal control and evolution strategy, to prove its wide applicability as L2 regularization. Besides, it will be interesting to combine UDUC with domain randomization methods, gathering both virtual and real multiple environmental interactions for a larger range of robustness.

Acknowledgements

This work is fully supported by the European Union’s Horizon 2020 research and innovation program under the Marie Skłodowska-Curie grant agreement No. 953348 (ELO-X).

References

- [1] J. Ackermann, A. Bartlett, D. Kaesbauer, W. Sienel, and R. Steinhauser. *Robust Control: Systems with Uncertain Physical Parameters*. Springer, 1993.
- [2] A. G. Barto, R. S. Sutton, and C. W. Anderson. Neuronlike adaptive elements that can solve difficult learning control problems. *IEEE transactions on systems, man, and cybernetics*, pages 834–846, 1983.
- [3] R. Bellman. A markovian decision process. *Journal of Mathematics and Mechanics*, 6(5):679–684, 1957. ISSN 0095-9057.
- [4] G. Brockman, V. Cheung, L. Pettersson, J. Schneider, J. Schulman, J. Tang, and W. Zaremba. Openai gym. *CoRR*, abs/1606.01540, 2016.
- [5] E. F. Camacho and C. B. Alba. *Model Predictive Control*. Springer Science & Business Media, Jan. 2013. ISBN 978-0-85729-398-5.
- [6] T. Chen, S. Kornblith, M. Norouzi, and G. Hinton. A simple framework for contrastive learning of visual representations. In *Proceedings of the 37th International Conference on Machine Learning*, pages 1597–1607. PMLR, Nov. 2020.
- [7] S. Chopra, R. Hadsell, and Y. LeCun. Learning a similarity metric discriminatively, with application to face verification. In *2005 IEEE Computer Society Conference on Computer Vision and Pattern Recognition (CVPR’05)*, volume 1, pages 539–546 vol. 1, June 2005. doi: 10.1109/CVPR.2005.202.
- [8] K. Chua, R. Calandra, R. McAllister, and S. Levine. Deep reinforcement learning in a handful of trials using probabilistic dynamics models. In *Advances in Neural Information Processing Systems*, volume 31. Curran Associates, Inc., 2018.
- [9] M. P. Deisenroth and C. E. Rasmussen. Pilco: A model-based and dataefficient approach to policy search. In *In Proceedings of the Twenty-Eighth International Conference on Machine Learning (ICML, 2011)*.
- [10] G. Dulac-Arnold, N. Levine, D. J. Mankowitz, J. Li, C. Paduraru, S. Gowal, and T. Hester. An empirical investigation of the challenges of real-world reinforcement learning, 2020.
- [11] B. Eysenbach, A. Gupta, J. Ibarz, and S. Levine. Diversity is all you need: Learning skills without a reward function. In *7th International Conference on Learning Representations, ICLR 2019, New Orleans, LA, USA, May 6-9, 2019*. OpenReview.net, 2019.
- [12] M. Gutmann and A. Hyvärinen. Noise-contrastive estimation: A new estimation principle for unnormalized statistical models. In *Proceedings of the Thirteenth International Conference on Artificial Intelligence and Statistics*, pages 297–304. JMLR Workshop and Conference Proceedings, Mar. 2010.
- [13] T. Haarnoja, A. Zhou, P. Abbeel, and S. Levine. Soft actor-critic: Off-policy maximum entropy deep reinforcement learning with a stochastic actor. In J. G. Dy and A. Krause, editors, *Proceedings of the 35th International Conference on Machine Learning, ICML 2018, Stockholm, Sweden, July 10-15, 2018*, volume 80 of *Proceedings of Machine Learning Research*, pages 1856–1865. PMLR, 2018.
- [14] K. He, H. Fan, Y. Wu, S. Xie, and R. Girshick. Momentum contrast for unsupervised visual representation learning. In *Proceedings of the IEEE/CVF Conference on Computer Vision and Pattern Recognition*, pages 9729–9738, 2020.
- [15] L. Hewing, K. P. Wabersich, M. Menner, and M. N. Zeilinger. Learning-based model predictive control: Toward safe learning in control. *Annual Review of Control, Robotics, and Autonomous Systems*, 3(1):269–296, 2020. doi: 10.1146/annurev-control-090419-075625.
- [16] G. N. Iyengar. Robust dynamic programming. *Mathematics of Operations Research*, 30(2):257–280, May 2005. ISSN 0364-765X, 1526-5471. doi: 10.1287/moor.1040.0129.
- [17] M. Janner, J. Fu, M. Zhang, and S. Levine. When to trust your model: Model-based policy optimization. In H. M. Wallach, H. Larochelle, A. Beygelzimer, F. d’Alché-Buc, E. B. Fox, and R. Garnett, editors, *Advances in Neural Information Processing Systems 32: Annual Conference on Neural Information Processing Systems 2019, NeurIPS 2019, December 8-14, 2019, Vancouver, BC, Canada*, pages 12498–12509, 2019.
- [18] S. Kariyappa and M. K. Qureshi. Improving adversarial robustness of ensembles with diversity training. *CoRR*, abs/1901.09981, 2019.
- [19] D. P. Kingma and J. Ba. Adam: A method for stochastic optimization. In Y. Bengio and Y. LeCun, editors, *3rd International Conference on Learning Representations, ICLR 2015, San Diego, CA, USA, May 7-9, 2015. Conference Track Proceedings*, 2015.
- [20] M. Laskin, A. Srinivas, and P. Abbeel. Curl: Contrastive unsupervised representations for reinforcement learning. In *Proceedings of the 37th International Conference on Machine Learning*, pages 5639–5650. PMLR, Nov. 2020.
- [21] Z. Liu, X. Li, B. Kang, and T. Darrell. Regularization matters in policy optimization - an empirical study on continuous control. In *9th International Conference on Learning Representations, ICLR 2021, Virtual Event, Austria, May 3-7, 2021*. OpenReview.net, 2021.
- [22] J. Moos, K. Hansel, H. Abdulsamad, S. Stark, D. Clever, and J. Peters. Robust reinforcement learning: A review of foundations and recent advances. *Machine Learning and Knowledge Extraction*, 4(1):276–315, Mar. 2022. ISSN 2504-4990. doi: 10.3390/make4010013.
- [23] A. Nagabandi, G. Kahn, R. S. Fearing, and S. Levine. Neural network dynamics for model-based deep reinforcement learning with model-free fine-tuning. In *2018 IEEE International Conference on Robotics and Automation, ICRA 2018, Brisbane, Australia, May 21-25, 2018*, pages 7559–7566. IEEE, 2018. doi: 10.1109/ICRA.2018.8463189.
- [24] A. Nagabandi, I. Clavera, S. Liu, R. S. Fearing, P. Abbeel, S. Levine, and C. Finn. Learning to adapt in dynamic, real-world environments through meta-reinforcement learning. In *7th International Conference on Learning Representations, ICLR 2019, New Orleans, LA, USA, May 6-9, 2019*. OpenReview.net, 2019.
- [25] X. B. Peng, M. Andrychowicz, W. Zaremba, and P. Abbeel. Sim-to-real transfer of robotic control with dynamics randomization. In *2018 IEEE International Conference on Robotics and Automation (ICRA)*, pages 3803–3810, May 2018. doi: 10.1109/ICRA.2018.8460528.
- [26] A. Rame and M. Cord. Dice: Diversity in deep ensembles via conditional redundancy adversarial estimation. In *International Conference on Learning Representations*, Oct. 2020.
- [27] A. Ross, W. Pan, L. Celi, and F. Doshi-Velez. Ensembles of locally independent prediction models. *Proceedings of the AAAI Conference on Artificial Intelligence*, 34(04):5527–5536, Apr. 2020. ISSN 2374-3468. doi: 10.1609/aaai.v34i04.6004.
- [28] R. Rubinfeld. The cross-entropy method for combinatorial and continuous optimization. *Methodology And Computing In Applied Probability*, 1(2):127–190, Sept. 1999. ISSN 1573-7713. doi: 10.1023/A:1010091220143.
- [29] J. Schulman, F. Wolski, P. Dhariwal, A. Radford, and O. Klimov. Proximal policy optimization algorithms. *CoRR*, abs/1707.06347, 2017.
- [30] R. S. Sutton and A. G. Barto. *Reinforcement Learning - an Introduction*. Adaptive Computation and Machine Learning. MIT Press, 1998. ISBN 978-0-262-19398-6.
- [31] A. Tuulpin and M. B. Blaschko. Greedy bayesian posterior approximation with deep ensembles. *Trans. Mach. Learn. Res.*, 2022, 2022.
- [32] E. Todorov, T. Erez, and Y. Tassa. Mujoco: A physics engine for model-based control. In *2012 IEEE/RSJ International Conference on Intelligent Robots and Systems*, pages 5026–5033, Vilamoura-Algarve, Portugal, Oct. 2012. IEEE. ISBN 978-1-4673-1736-8 978-1-4673-1737-5 978-1-4673-1735-1. doi: 10.1109/IROS.2012.6386109.
- [33] A. van den Oord, Y. Li, and O. Vinyals. Representation learning with contrastive predictive coding. *CoRR*, abs/1807.03748, 2018.
- [34] D. Wang and Q. Liu. Nonlinear stein variational gradient descent for learning diversified mixture models. In *Proceedings of the 36th International Conference on Machine Learning*, pages 6576–6585. PMLR, May 2019.
- [35] T. Wang, X. Bao, I. Clavera, J. Hoang, Y. Wen, E. D. Langlois, S. Zhang, G. Zhang, P. Abbeel, and J. Ba. Benchmarking model-based reinforcement learning. *CoRR*, abs/1907.02057, 2019.
- [36] W. Wiesemann, D. Kuhn, and B. Rustem. Robust markov decision processes. *Mathematics of Operations Research*, 38(1):153–183, Feb. 2013. ISSN 0364-765X. doi: 10.1287/moor.1120.0566.
- [37] J. Wu, J. Chen, J. Wu, W. Shi, X. Wang, and X. He. Understanding contrastive learning via distributionally robust optimization. In *Thirty-Seventh Conference on Neural Information Processing Systems*, Nov. 2023.
- [38] Y. Zhang, J. Wang, and J. Boedecker. Robust reinforcement learning in continuous control tasks with uncertainty set regularization. In *7th Annual Conference on Robot Learning*, Aug. 2023.

UDUC: An Uncertainty-driven Approach for Learning-based Robust Control (Supplementary Material)

A Additional Algorithm Details

A.1 Proof of Proposition 1

In the case of UDUC loss, we first denote the training environment's transition distribution $\mathcal{T}_{\text{train}}(s'|s, a)$ ($\mathcal{T}_{\text{train}}$ in short), possible testing environment's transition distribution $\mathcal{T}_{\text{test}}(s'|s, a)$ ($\mathcal{T}_{\text{test}}$ in short) and probabilistic ensemble functions with target parameters $f(s'|s, a; \theta) = \frac{1}{B} \sum_{b=1}^B f_b(s'|s, a; \bar{\theta}_b)$. We formally formulate a robust optimization problem and prove its equivalence to UDUC loss (Equation 3) in the following Proposition.

Proposition 1 (Understanding UDUC loss). *Minimizing UDUC loss is equivalent to a robust optimization problem:*

$$\begin{aligned} \min_{\theta_b} \mathcal{L}_{\text{RO}}(\theta_b, s, a) &= \min_{\theta_b} \left(1 - \frac{1}{\tau} \underbrace{\mathbb{E}_{s' \sim \mathcal{T}_{\text{train}}} [\mathcal{L}_{\text{PE}}(\theta_b, s, a, s')] }_{\text{negative log-likelihood term}} \right) + \frac{1}{\tau} \underbrace{\left(\mathbb{E}_{s' \sim f(s'|s, a; \bar{\theta})} [-\mathcal{L}_{\text{PE}}(\theta_b, s, a, s')] - \max_{\mathcal{T}_{\text{test}}} \mathbb{E}_{s' \sim \mathcal{T}_{\text{test}}} [-\mathcal{L}_{\text{PE}}(\theta_b, s, a, s')] \right)}_{\text{regularization term}} \\ \text{s.t. } D_{\text{KL}}(\mathcal{T}_{\text{test}} \|\mathcal{T}_{\text{train}}) &\leq \eta, \eta \approx \mathbb{V}_{s' \sim f(s'|s, a)} [\mathcal{L}_{\text{PE}}(\theta_b, s, a, s')] / 2\tau^2, \end{aligned}$$

where $\mathcal{L}_{\text{RO}}(\theta_b, s, a)$ is the target of this robust optimization problem, consisting of a negative log-likelihood term and a regularization term.

Proof. Rethinking UDUC loss in Equation 3 $\mathcal{L}_{\text{UDUC}}(\theta_b, s, a, \mathcal{X}) = (1 - \frac{1}{\tau}) \mathcal{L}_{\text{PE}}(\theta_b, s, a, s'_b) + \mathcal{L}_{\text{InfoNCE}}(\theta_b, s, a, \mathcal{X})$, we can first rewrite it into the expectation form as $\mathcal{L}_{\text{UDUC-e}}(\theta_b, s, a) = (1 - \frac{1}{\tau}) \mathcal{L}_1(\theta_b, s, a) + \mathcal{L}_2(\theta_b, s, a)$ where $\mathcal{L}_1(\theta_b, s, a) = \mathbb{E}_{s' \sim \mathcal{T}_{\text{train}}} [\mathcal{L}_{\text{PE}}(\theta_b, s, a, s')]$ and $\mathcal{L}_2(\theta_b, s, a) = \mathbb{E}_{s^+ \sim \mathcal{T}_{\text{train}}, s^- \sim f(s'|s, a; \bar{\theta})} [\mathcal{L}_{\text{InfoNCE}}(\theta_b, s, a, \mathcal{X})]$. Notably, $\mathcal{L}_1(\theta_b, s, a)$ is the same as the negative log-likelihood term in $\mathcal{L}_{\text{RO}}(\theta_b, s, a)$. Therefore, we only need to prove that $\min \mathcal{L}_2(\theta_b, s, a)$ is equivalent to the reduced optimization problem as follows:

$$\begin{aligned} \min_{\theta_b} \mathcal{L}_{\text{RO-r}}(\theta_b, s, a) &= \min_{\theta_b} \frac{1}{\tau} \underbrace{\left(\mathbb{E}_{s' \sim f(s'|s, a; \bar{\theta})} [-\mathcal{L}_{\text{PE}}(\theta_b, s, a, s')] - \max_{\mathcal{T}_{\text{test}}} \mathbb{E}_{s' \sim \mathcal{T}_{\text{test}}} [-\mathcal{L}_{\text{PE}}(\theta_b, s, a, s')] \right)}_{\text{regularization term}} \\ \text{s.t. } D_{\text{KL}}(\mathcal{T}_{\text{test}} \|\mathcal{T}_{\text{train}}) &\leq \eta, \eta \approx \mathbb{V}_{s' \sim f(s'|s, a)} [\mathcal{L}_{\text{PE}}(\theta_b, s, a, s')] / 2\tau^2, \end{aligned} \quad (4)$$

where $\mathcal{L}_{\text{RO-r}}(\theta_b, s, a)$ only preserves the regularization term in $\mathcal{L}_{\text{RO}}(\theta_b, s, a)$.

We can further rewrite $\mathcal{L}_2(\theta_b, s, a)$ in the following way:

$$\begin{aligned} \mathcal{L}_2(\theta_b, s, a) &= \mathbb{E}_{s^+ \sim \mathcal{T}_{\text{train}}, s^- \sim f(s'|s, a; \bar{\theta})} [\mathcal{L}_{\text{InfoNCE}}(\theta_b, s, a, \mathcal{X})] \\ &= -\log \mathbb{E}_{s^+ \sim \mathcal{T}_{\text{train}}} [\exp(-\mathcal{L}_{\text{PE}}(\theta_b, s, a, s^+) / \tau)] + \log \mathbb{E}_{s^- \sim f(s'|s, a; \bar{\theta})} [\exp(-\mathcal{L}_{\text{PE}}(\theta_b, s, a, s^-) / \tau)] \\ &= -\left[-\log \mathbb{E}_{s^+ \sim f(s'|s, a; \bar{\theta})} [\exp(-\mathcal{L}_{\text{PE}}(\theta_b, s, a, s^+) / \tau)] + \log \mathbb{E}_{s^- \sim \mathcal{T}_{\text{train}}} [\exp(-\mathcal{L}_{\text{PE}}(\theta_b, s, a, s^-) / \tau)] \right] \\ &= -\mathcal{L}_{\text{InfoNCE-alt}}(\theta_b, s, a). \end{aligned}$$

Therefore, minimizing $\mathcal{L}_2(\theta_b, s, a)$ is equivalent to maximizing another InfoNCE-styled loss $\mathcal{L}_{\text{InfoNCE-alt}}(\theta_b, s, a)$, where positive samples are drawn from $f(s'|s, a; \bar{\theta})$ and negatives from $\mathcal{T}_{\text{train}}$. The following proof is built on the previous work [37] that has shown the equivalence between InfoNCE loss and robust the outcome of an optimization as follows:

Theorem 1 (CL-RO Equivalence [37]). *For the expected version of InfoNCE loss $\mathcal{L}_{\text{InfoNCE-e}}(\theta, c) = -\log \frac{\mathbb{E}_{x^+ \sim p(x^+|c)} [\exp(g_\theta(x, c)/\tau)]}{\mathbb{E}_{x^- \sim q(x^-)} [\exp(g_\theta(x^-, c)/\tau)]}$, it is equivalent to the outcome of an optimization problem:*

$$\mathcal{L}_{\text{opt}}(\theta, c) = \max_z -\mathbb{E}_{x \sim p(x|c)} [g_\theta(x, c)] / \tau + \mathbb{E}_{x \sim z(x)} [g_\theta(x, c)] / \tau, \quad \text{s.t. } D_{\text{KL}}(z \| q) \leq \eta,$$

with the relation as $\mathcal{L}_{\text{opt}}(\theta, c) = \mathcal{L}_{\text{InfoNCE-e}}(\theta, c) + \text{const}$, $\tau \approx \sqrt{\mathbb{V}_{x \sim q(x)} [g_\theta(x, c)] / 2\eta}$.

In the case of the MDP formulation, the context c is actually the state and action pair (s, a) , the next state s' as the sample x and the representation function $g_{\theta_b}(x, c) = -\mathcal{L}_{\text{PE}}(\theta_b, s, a, s')$. The positive distribution $p(x|c)$ is equivalent to probabilistic ensemble functions with target parameters $f(s'|s, a; \bar{\theta}) = \frac{1}{B} \sum_{b=1}^B f_b(s'|s, a; \bar{\theta}_b)$ and the negative distribution $q(x)$ comes from the training transition distribution $\mathcal{T}_{\text{train}}(s'|s, a)$. According to the Theorem 1, the alternative InfoNCE loss $\mathcal{L}_{\text{InfoNCE-alt}}(\theta_b, s, a)$ can be transformed into the outcome of an optimization problem such that:

$$\mathcal{L}_{\text{opt}}(\theta_b, s, a) = -\frac{1}{\tau} \mathbb{E}_{s' \sim f(s'|s, a; \bar{\theta})} [-\mathcal{L}_{\text{PE}}(\theta_b, s, a, s')] + \max_{\mathcal{T}_{\text{test}}} \frac{1}{\tau} \mathbb{E}_{s' \sim \mathcal{T}_{\text{test}}} [-\mathcal{L}_{\text{PE}}(\theta_b, s, a, s')] \quad \text{s.t. } D_{\text{KL}}(\mathcal{T}_{\text{test}} \|\mathcal{T}_{\text{train}}) \leq \eta.$$

Consequently, minimizing $\mathcal{L}_2(\theta_b, s, a)$ is equivalent to maximizing $\mathcal{L}_{\text{opt}}(\theta_b, s, a)$. This can be further transformed into minimizing $-\mathcal{L}_{\text{opt}}(\theta_b, s, a)$, which is exactly the case of $\min_{\theta_b} \mathcal{L}_{\text{RO-r}}(\theta_b, s, a)$. □

A.2 Control with Probabilistic Ensemble Functions

A.2.1 Model Predictive Control

Given a transition function $f(s'|s, a; \theta)$, deriving the policy $\pi(a|s)$ in the MPC is an optimization problem. To better handle the computational efficiency, cross-entropy-based methods [28] are often considered. We detail the procedures in Algorithm 2 to generate controls with the learned ensemble function. In basic, the learned transition functions are used to generate trajectories for optimization. For each step, one ensemble member is randomly sampled, which ensures the multi-mode prediction in the next states and promotes robustness. The other propagation method is introduced in Chua et al. [8].

Algorithm 2 Cross-Entropy with Probabilistic Ensembles

```

1: Input: Ensemble transition function  $f(s'|s, a; \theta)$  with parameters  $\theta = \{\theta_1, \dots, \theta_B\}$ , policy function  $\pi(a|s)$ , environment dataset  $\mathcal{D}_{\text{env}} = \{\}$ ,
   model dataset  $\mathcal{D}_{\text{model}} = \{\}$ , target update rate  $\rho$ , initial state  $s$ , model-agent update frequency  $F_{\text{model}}, F_{\text{agent}}$ , population size  $N$ , elite size  $K$ ,
   horizon  $H$ , action dimension  $A$ 
2: Set target transition function's parameters  $\bar{\theta} \leftarrow \theta$ 
3: Set initial cross-entropy parameters  $\mu \leftarrow [0, \dots, 0]^T : \mathbb{R}^{H \times A}$  the mean and  $\Sigma \leftarrow I : (\mathbb{R}^{H \times A})^2$  the variance
4: for steps  $i = 1, 2, \dots$  do
5:   for iterations  $j = 1, 2, \dots$  /*run cross-entropy*/ do
6:     Generate  $N$  samples  $X_{1:N} \sim \mathcal{N}(\mu, \Sigma)$ 
7:     for sample  $n = 1, 2, \dots, N$  do
8:       Rollout a trajectory  $(s_1, a_1, \dots, s_H, a_H)$ , where  $a_t$  is directly accessed from  $X_n[(t-1) * H : t * H]$ , and  $s_{t+1}$  sampled from
          $f_b(s'|s, a; \theta_b)$  where  $b$  is a random select ensemble member.
9:       Calculate score  $S_n \leftarrow [\exp(-\sum_{t=1}^H r(s_t, a_t))]$ 
10:    end for
11:     $X_{1:N} \leftarrow \text{sort}(X_{1:N})$  depending on  $S_{1:N}$ 
12:     $\mu \leftarrow \text{mean}(X_{1:K})$ 
13:     $\Sigma \leftarrow \text{var}(X_{1:K})$ 
14:  end for
15:  Execute  $a = \mu$  in the training environment
16:  Observe reward  $r$  and next state  $s'$ 
17:   $\mathcal{D}_{\text{env}} \leftarrow \mathcal{D}_{\text{env}} \cup \{s, a, r, s'\}$  and  $s \leftarrow s'$ 
18:  if  $i \bmod F_{\text{model}} \equiv 0$  /*update model*/ then
19:    Update parameters  $\theta$  by minimizing Equation 3
20:    Update target parameters  $\bar{\theta} \leftarrow (1 - \rho)\bar{\theta} + \rho\theta$ 
21:    Rollout transitions  $(s_n, a_n, r_n, s_{n+1})_{n=1}^N$  with  $f(s'|s, a; \bar{\theta})$ ,  $\pi(a|s)$  and  $r(s, a)$ 
22:    Store in the model dataset  $\mathcal{D}_{\text{model}} \leftarrow \mathcal{D}_{\text{model}} \cup \{(s_n, a_n, r_n, s_{n+1})_{n=1}^N\}$ 
23:  end if
24: end for

```

A.2.2 Reinforcement Learning

For RL, the policy $\pi(a|s)$ is usually modelled as a neural network. The policy can be improved with actor-critic frameworks. Soft Actor Critic (SAC) [13] is one of the state-of-the-art algorithms in the field. We detail the procedures in Algorithm 3 to learn $\pi(a|s)$ with the learned ensemble function. In basic, the learned transition functions are used to generate transitions (s, a, s') and further stored in the dataset $\mathcal{D}_{\text{model}}$. SAC uses this data to update critic and actor parameters. The specific loss function $J_Q(\theta)$ $J_\pi(\phi)$ can be referred in Haarnoja et al. [13].

B Additional Experimental Setups

B.1 Introduction on Robots and Tasks

In this paper, the experiments mainly touch on 3 different robots, the cart-pole, the walker and the humanoid. These 3 robots are visualized in Figure 7. The introduction of these robots is as follows:

- **Cart-pole** has an un-actuated pole on top of a moving cart. The `cartpole_balance` task aims to balance the pole on the origin position with a horizontal force on the cart.
- **Walker** is a planar walker to be controlled in 6 dimensions. The `walker_stand` task requires an upright torso and some minimal torso height. The `walker_walk` task encourages a forward velocity.
- **Humanoid** is a generic humanoid robot with a more complex state and action space than the cart-pole and the walker. The `humanoid_walk` tasks encourage a level of forward speed.

The specific reward function can be found in the original work of RWRL [10]. Here, we set the maximum episode length as 1000 for the walker and humanoid, and 100 for the cart-pole. Therefore, the maximum possible episode reward is 1000, 5000, 100 respectively.

Algorithm 3 Soft Actor Critic with Probabilistic Ensembles

- 1: **Input:** Double action value $Q(s, a; \theta)$ with parameters θ_1^Q, θ_2^Q ensemble transition function $f(s'|s, a; \theta)$ with parameters $\theta = \{\theta_1, \dots, \theta_B\}$, policy function $\pi(a|s)$, environment dataset $\mathcal{D}_{\text{env}} = \{\}$, model dataset $\mathcal{D}_{\text{model}} = \{\}$, target update rate ρ , initial state s , model-agent update frequency F_{model} and F_{agent} , SAC's learning rate for critic and actor network λ_Q, λ_π , and target network update ratio τ
 - 2: Set target transition function's parameters $\bar{\theta} \leftarrow \theta$
 - 3: **for** steps $i = 1, 2, \dots$ **do**
 - 4: Execute $a \sim \pi(a|s)$ in the training environment
 - 5: Observe reward r and next state s'
 - 6: $\mathcal{D}_{\text{env}} \leftarrow \mathcal{D}_{\text{env}} \cup \{s, a, r, s'\}$ and $s \leftarrow s'$
 - 7: **if** $i \bmod F_{\text{model}} \equiv 0$ */*update model*/* **then**
 - 8: Update parameters θ by minimizing Equation 3
 - 9: Update target parameters $\bar{\theta} \leftarrow (1 - \rho)\bar{\theta} + \rho\theta$
 - 10: Rollout transitions $(s_n, a_n, r_n, s_{n+1})_{n=1}^N$ with $f(s'|s, a; \bar{\theta}), \pi(a|s)$ and $r(s, a)$
 - 11: Store in the model dataset $\mathcal{D}_{\text{model}} \leftarrow \mathcal{D}_{\text{model}} \cup \{(s_n, a_n, r_n, s_{n+1})_{n=1}^N\}$
 - 12: **end if**
 - 13: **if** $i \bmod F_{\text{agent}} \equiv 0$ */*update agent*/* **then**
 - 14: $\theta_i \leftarrow \theta_i - \lambda_Q \hat{\nabla}_{\theta_i} J_Q(\theta_i)$ for $i \in \{1, 2\}$
 - 15: $\psi \leftarrow \psi - \lambda_\pi \hat{\nabla}_\psi J_\pi(\psi)$
 - 16: $\bar{\theta}_i \leftarrow \tau\theta_i + (1 - \tau)\bar{\theta}_i$ for $i \in \{1, 2\}$
 - 17: **end if**
 - 18: **end for**
-



(a) Cart-pole

(b) Walker

(c) Humanoid

Figure 7: Visualization of 3 robots used in the experiments.

B.2 Hyperparameters for RWRL

For RWRL tasks, we learn a probabilistic ensemble model and use the model to train a neural network agent with the SAC algorithm in RL. The model has the structure of a feed-forward neural network to predict the mean and variance of the delta states. For the SAC agent, we adopt the double critic technique and with the agent generating a Gaussian control. To compare all algorithms fairly, we set the model structures and hyperparameters equally, except for the regularization coefficients for different algorithms. All algorithms are trained with Adam optimizer [19]. The full hyperparameters are shown in Table 2. For regularization coefficients, we manually tune them for each algorithm by increasing their values until the control performance on the nominal environment drops, and the values range in $\{0, 1e-6, 1e-5, 1e-4, 1e-3, 1e-2, 1e-1, 1e0\}$. The specific values can be found in Table 3. In the future, it can be automatically tuned by learning a non-regularized control policy and comparing the control performance between these agents. All experiments are carried out on NVIDIA GeForce RTX 2080 Ti and Pytorch 1.10.1.

B.3 Hyperparameters for Cart-pole

For the cart-pole balance task, instead, we learn a physical-based ensemble model with parameters pole mass and pole length and use the model to drive a CEM controller in the MPC style. For the model, it has the structure of a feed-forward neural network to predict the mean of the next states. The full hyperparameters are shown in Table 4.

C Additional Experimental Results

C.1 Training Performances

We provide additional training results regarding the neg log-likelihood, regularization, gradients norm and model training dataset. From the neg log-likelihood, we can see UDUC loss learns slower on the nominal model compared with other baselines, proving the contrastive loss is

Table 2: Hyperparameters for RWRL tasks.

Hyperparameters	walker_stand	walker_walk	humanoid_walk
max training steps	2e5	2e5	2e5
episode length	1e3	1e3	1e3
dynamics network	4x MLP(200)	4x MLP(200)	4x MLP(200)
number of ensembles	5	5	7
propagation method	random	random	random
activation function	SiLU	SiLU	SiLU
model learning rate	3e-4	3e-4	3e-4
model batch size	256	256	256
model update frequency	250	250	250
effective model rollouts per step	400	400	400
rollout schedule	[20,150,1,1]	[20,150,1,1]	[20,300,1,25]
<i>/*for SAC agent*/</i>			
critic network	2 x MLP(1024)	2x MLP(1024)	2x MLP(1024)
actor network	2x 1024	2x 1024	2x 1024
discount factor γ	0.99	0.99	0.99
init temperature	1.0	1.0	1.0
temperature learning rate	3e-3	3e-3	1e-4
actor learning rate	3e-4	3e-4	1e-4
actor update frequency	4	4	1
critic learning rate	3e-4	3e-4	1e-4
critic update frequency	1	1	1
critic target update rate	0.005	0.005	0.005
critic target update frequency	4	4	4
sac updates per step	20	20	20
epochs to retain sac buffer	1	1	5
sac batch size	256	256	256
target entropy	-3	-3	-1

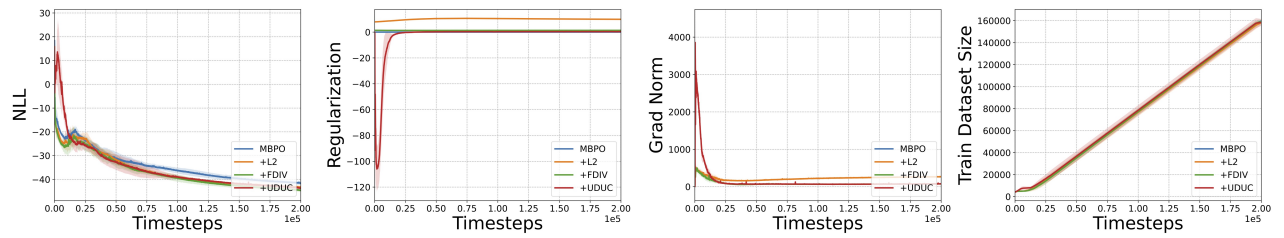
Table 3: Regularization coefficients for all baseline methods.

Task Name	Algorithms			
	MBPO	+L2	+FDIV	+UDUC
walker_stand	-	1e-1	1e-2	1e-2
walker_walk	-	1e-2	1e-3	1e-3
humanoid_walk	-	1e-2	1e-4	1e-3

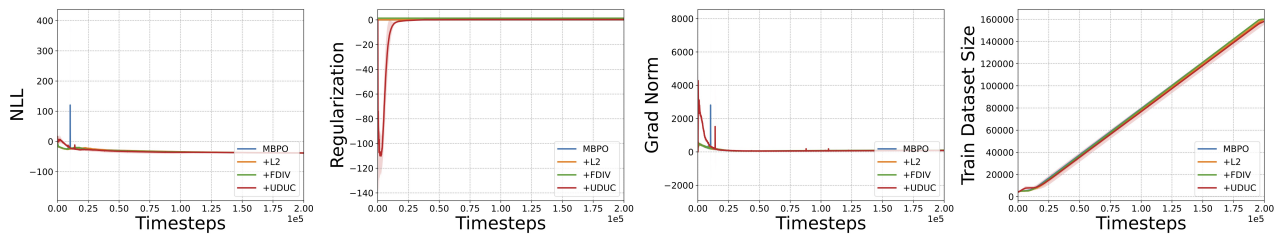
Table 4: Hyperparameters for cart-pole balance task.

Hyperparameters	cartpole_balance
max training steps	500
episode length	100
number of ensembles	9
propagation method	random
<i>/*for CEM agent*/</i>	
model learning rate	1e-3
model batch size	32
model update frequency	100
planning horizon	15
replan frequency	1
optimization iterations	5
elite ratio	0.1
population size	500
particles	20

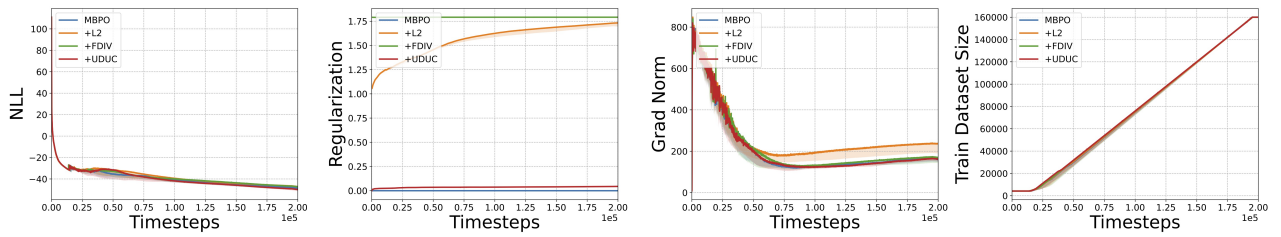
working at the beginning. This phenomenon is more obvious from the regularization and grad norm figure of the walker robot. For the figure of the size of the training dataset is to show that all models are trained on the same amount of data.



(a) walker_stand



(b) walker_walk



(c) humanoid_walk

Figure 8: Additional training curves on robot control tasks. The x-axis is the environment time steps and the y-axis is neg log-likelihood, regularization, gradients norm and model training dataset. All graphs are plotted with median and 25%-75% percentile shading across 5 random seeds.